Journal of Thermal Analysis, Vol. 36 (1990) 1171-1189

AN APPRECIATION OF USABILITY OF THE FINITE ELEMENT METHOD FOR THE THERMAL ANALYSIS OF STRIPE-GEOMETRY DIODE LASERS

R. P. Sarzala and *W. Nakwaski*

INSTITUTE OF PHYSICS, TECHNICAL UNIVERSITY OF LÓDZ, ul. WOLCZANSKA 219, 93-005 LODZ, POLAND

(Received November 7, 1989)

An appreciation of usability of the finite element technique for the thermal analysis of stripe-geometry diode lasers is carried out in the present work. Thye technique appears to be very exact and surprisingly speed using even a standard IBM PC/AT microcomputer.

As an example, a finite-element thermal analysis of the diffused-stripe double-heterostructure GaAs/(AlGa)As diode laser is carried out. A system of isotherms obtained for the above laser enables us to discuss the heat spreading process within its structure and to compare relative contributions of all heat sources.

An operation of diode lasers (DLS) strongly depends on their thermal properties because all electrical and optical processes taking place inside a DL crystal are temperature-dependent. Consequently all DL operation characteristics are sensitive to a temperature distribution within and around a DL active area. Therefore thermal properties of diode lasers are of prime importance.

Up to now experimental methods determining temperature profiles within the DL crystal with a required space resolution and a necessary temperature exactness have not been found. Therefore theoretical thermal modelling of diode lasers remains the most useful tool for such an application.

Most of thermal models [1-7] of stripe-geometry diode lasers are based on the classical semi-analytical thermal analysis of the diffused-stripe diode lasers reported by Joyce and Dixon [8]. There are also known fully analytical thermal DL models for a steady state cw operation [9, 10], a transient-state pulse operation [11] and self-cooling of the DL crystal between the current pulses [12].

John Wiley & Sons, Limited, Chichester
Akadémiai Kiadó, Budapest

An analytical solving of the nonlinear thermal conduction equation requires some approximations which may impose severe restrictions on the versatility and range of validity of the model. Therefore some finite-difference numerical thermal models [13-15] of stripe-geometry diode lasers have been also proposed. The above models require however long computing times of powerful computers. Therefore the modern finite-element technique should be tested for such an application. First attempts [16, 17] gave promising results but in our opinion they did not show all advantages of the method.

The paper has the purpose of carrying out an appreciation of usability of the finite element method (FEM) [18] for the thermal analysis of stripe-geometry diode lasers. The method will be tested in Section 2 for the broad-contact diode lasers (for which the simple analytical solutions are known) to determine its temperature accuracy. Afterwards the method will be applied in Section 3 to diffused-stripe diode lasers to determine the required central processing unit (CPU) times of calculations for the standard IBM PC/AT computer.

The accuracy of the finite-element technique in temperature calculations for diode lasers

The broad-contact (BC) diode lasers

The best way to determine the exactness of a numerical technique is to compare its results with those obtained with the aid of a known analytical solution. Let us choose to this end two simple laser structures, namely the broad-contact homojunction (HJ) GaAs diode laser and the broad-contact double-heterostructure (DH) GaAs/(AlGa)As diode laser, for which analytical solutions of temperature distributions exist in a scientific literature [19, 20]. Constructions of both the HJ and the DH lasers are explained schematically in Figs 1 and 2, respectively, where also some construction parameters and thermal conductivities of all semiconductor layers are indicated.

Let us consider the main heat source of a diode laser placed in the active area and connected mainly with nonradiative recombination (c. f. Section 3.2). All other heat sources are neglected here because we are not going to carry out a detailed thermal analysis of the above broad contact lasers because these unmodern devices went out of use already but only to appreciate the exactness of the finite-element technique for this application. The heat

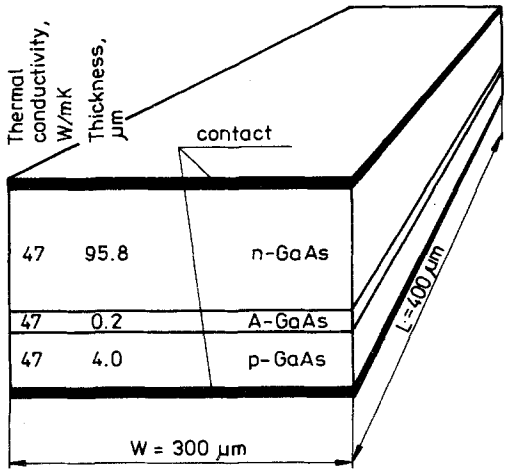

Fig. 1 The broad-contact homojunction (HJ) GaAs diode laser. Not to scale. A - active layer, L and W - length and width of the DL crystal

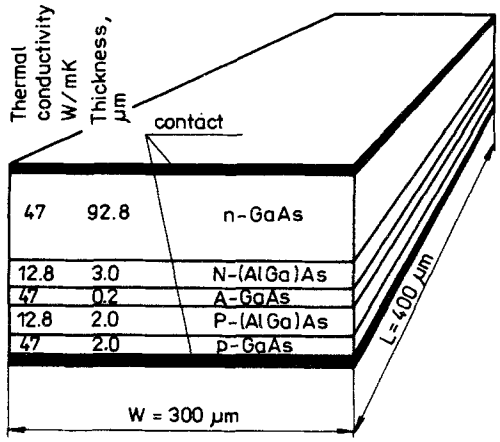

Fig. 2 The broad-contact double-heterostructure (DH) GaAs/(AlGa)As diode laser. Not to scale. A - active layer, L and W - legth and width of the DL crystal

generation rate is assumed to be $g = 8.26.10^{14}$ W/m^3. The same value is used for both the laser constructions to compare by the way efficiencies of their heat sinking mechanisms. In real structures, the heat generation rate should be much higher for the HJ laser in the case of which the continuous wave (cw) operation has not been achieved yet at room temperature of the am-

bient. For a typical value of the external quantum efficiency a_D = 30 %., the above heat generation rate corresponds for the structures under consideration (c. f. Fig. 1 and Fig. 2) to the supply current c. a. 20 A and to the supply current density c. a. 16.500 A/cm^2.

As usually, we neglect all the heat sinking mechanisms but the most efficient one, i. e. the conduction through a bottom contact to a heat sink. Therefore equivalent thermal schemes of the lasers under consideration may be shown in a form presented in Fig. 3.

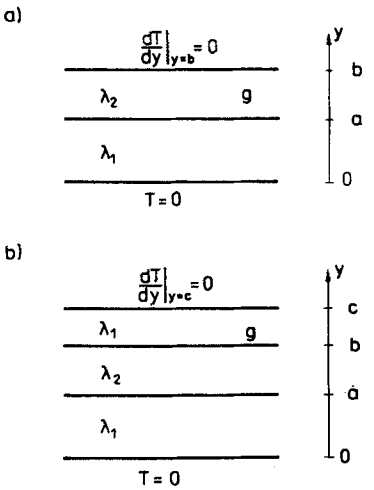

Fig. 3 The equivalent thermal schemes of the broad contact diode lasers: a) the homojunction laser, b) the double-heterostructure laser, λ_1 and λ_2 - thermal conductivities, g - heat generation rate, a, b - a and c - b - thicknesses of the layers

Analytical temperature distributions in the BC diode lasers

The temperature distributions may be now expressed in the following forms [20]:

a) for the HJ laser:

$$T(y) = \begin{cases} g(b-a)y/\lambda, & \text{for } y \in [0,a] \\ -(g/2\lambda_2)(y-a)^2 + (g/\lambda_2)(b-a)(y-a) + \\ +(g/\lambda_1)(b-a)a & \text{for } y \in [a,b] \end{cases} \quad (1)$$

b) for the DH laser:

$$T(y) = \begin{cases} g(c-b)y/\lambda_1 & \text{for } y \in [0,a] \\ g(c-b)[a/\lambda_1 + (y-a)/\lambda_2] & \text{for } y \in [a,b] \\ -(g/2\lambda_1)(y-b)^2 + (g/2\lambda_1)(c-b)(y-b) + & \\ + g(c-b)[a/\lambda_1 + (b-a)/\lambda_2] & \text{for } y \in [b,c] \end{cases} \quad (2)$$

For the HJ laser. both the thermal conductivities are equal to that of GaAs, i. e. $\lambda_1 = \lambda_2 = 47$ W/mK, whereas for the DH laser: $\lambda_1 = 47$ W/mK and $\lambda_2 = 12.8$ W/mK. The values of the thermal conductivities have been taken from References [21-24].

Numerical temperature distributions in the BC diode lasers

In the numerical calculations, the FEM software module O.K.FOUR has been used. Both of the laser structures have been covered with the grid of 360 perpendicular elements and 400 nodes. The CPU time required for this program has been equal to about 50 seconds for the IBM PC/AT (6 MHz) microcomputer.

Table 1 Distributions of temperature increments within the HJ and the DH broad-contact lasers for cw operation

y,	Temperature increment, K	
μm	HJ laser	DH laser
0.0	0.0	0.0
0.2	0.7	0.7
1.0	3.5	3.5
1.8	6.3	6.3
2.0	7.0	7.0
2.2	7.8	9.6
3.0	10.6	20.0
3.8	13.4	30.3
4.0	14.1	32.9
4.1	14.4	33.2
4.2	14.4	33.3

Results of the calculations are listed in Table 1. For both the laser structures, results of the FEM numerical calculations are completely identical with those of analytical ones. On the basis of the above facts, we may consider the finite element method to be a very exact and speed numerical technique in the temperature calculations for the diode lasers. Therefore we may conclude that the FEM technique satisfies all our requirements to be a

powerful tool in the thermal analysis of diode lasers. Its application for the diffused-stripe diode laser will be presented in the next Section.

By the way, we can compare the effectivenesses of the heat-sinking mechanisms in both the laser structures under consideration. As it can be seen from Table 1, in the HJ laser structure, heat is removed from the active area much more efficiently. On the other hand, however, the DH lasers are known to have much better thermal properties, they can operate efficiently even at relatively high temperatures of the ambient [25, 26] whereas the highest temperature of the ambient for which a cw operation of the HJ laser has been achieved is relatively low, $T_{A,HJ} = 202.5$ K [27]. It is because the threshold current of the homojunction laser is much higher than that of the DH laser and consequently real values of the heat generation rate are considerably higher in the former device.

Table 2 Nominal set of the parameters used for temperature calculations for the diffused-stripe DH GaAs/(AlGa)As diode laser

Parameter	Symbol	Value
Ambient temperature	T_A	300 K
Supply current	I	1 A
Threshold current	I_{TH}	100 mA
Voltage drop at the p-n junction	U	1.43 V
Quantum efficiencies:		
- internal, spontaneous emission	a_{SP}	0.55
- internal, lasing	a_i	1
- differential external, lasing	a_E	0.3
Difference of an AlAs content between the passive and the active layers	Δx	0.3
Thickness of the absorbing layer in the substrate	d'_N	1 μm

Finite element thermal analysis of the diffused-stripe diode laser

A typical construction of the diffused-stripe DH GaAs/(AlGa)As diode laser is schemetically shown in Fig. 4, where also thicknesses of the semiconductor layers and their thermal conductivities [21-24] are given. Contacting system of the laser is explained in Fig. 5. Thermal conductivities of the metallic layers have been taken from Ref. [28].

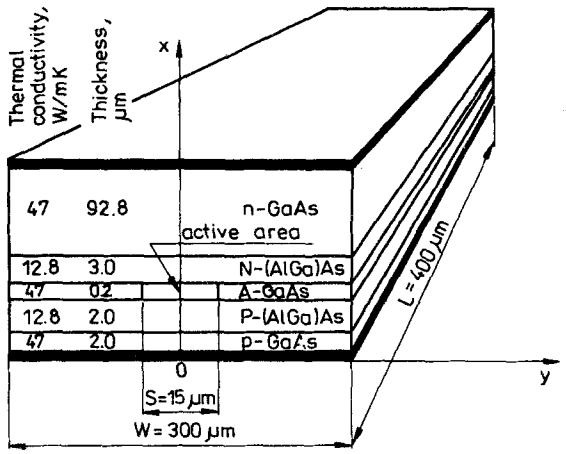

Fig. 4 The diffused-stripe double-heterostructure (DH) GaAs/(AlGa)As diode laser. Not to scale. A - active area, L and W - length and width of the DL crystal, S - stripe width. The coordinate system is also shown

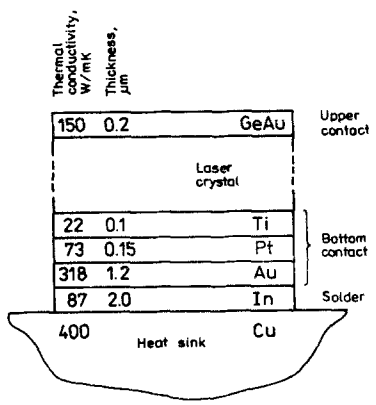

Fig. 5 Contacts of the DH stripe-geometry laser under consideration. Not to scale

Heat sources

The most efficient heat source in a diode laser is connected mainly with nonradiative recombination, and also with reabsorption of radiation. This source is placed in the active region and its heat generation rate may be expressed as [29]

$$g_A = (U/d)\{j_{TH}(1\text{-}fa_{SP}) + (j\text{-}j_{TH})[1\text{-}a_E\text{-}(1\text{-}a_i)a_{SP}f]\} \quad (3)$$

where d is the active layer thickness, U is the voltage drop at the p-n junction; j and j_{TH} are the supply current density and the threshold current density, respectively; a_{SP}, a_E and a_i are the internal quantum efficiency of the spontaneous emission, the external differential quantum efficiency of the lasing and the internal quantum efficiency of the lasing, respectively.

Coefficient f describes a fraction of the spontaneous emission from the active area which is transferred radiatively through the wide-gap passive (AlGa)As layers and may be expressed as follows [30]:

$$f = 2\sin^2[0.5\text{arc}\sin(1\text{-}0.62\Delta x/n_R)] \quad (4)$$

where $n_R = 3.59$ is the refractive index of the active layer material and Δx is the difference of an AlAs content between passive and active layers.

The spontaneous radiation transferred through the passive layers is absorbed in the capping p-type GaAs layer as well as in the lower part (the T layer of a thickness d'_N) of the n-type GaAs substrate. Corresponding heat generation rates are equal to:

$$g_{T,P} = Uj_{TH}a_{SP}/(2d_P) \quad (5)$$

$$g_{T,N} = Uj_{TH}a_{SP}f/(2d'_N) \quad (6)$$

where d_P is the p-GaAs layer thickness.

The Joule heating is generated in each layer with a density

$$g_{J,i} = j^2\rho_i \quad (7)$$

where ρ_i is the electrical resistivity of the ith layer.

All heat generation rates considered in the model are listed in Table 3 (electrical resistivities are taken from Table 4). As one can see, the dominating heat source is placed in the active area. Absorption of the spontaneous radiation transferred radiatively from the active area and Joule heating in the p-GaAs, N-(AlGa)As and P-(AlGa)As layers play supplementary role in the heating process. In imperfect structures, the Joule heat source within the contact layers, mainly the p-side contact heating, is also of some importance [15, 17].

Table 3 Heat generation rates in the considered diffused-stripe diode laser supplied with the current $I = 1\,A$

Mechanism	Place	Generation rate, 10^{12}W/m^3	Heat power, mW
Nonradiative recombination and reabsorption of radiation	Active area	825.2	990.2
Absorption of spontaneous radiation transferred radiatively through passive layers	p-GaAs	2.2	27.0
	lower part of the substrate	4.5	27.0
Joule heating	p-GaAs	5.6	67.2
	N-(AlGa)As	11.4	205.2
	P-(AlGa)As	2.0	24.0

Table 4 Values of doping concentrations and electrical resistivities of the semiconductor layers

Layer	Doping, 10^{10}cm^3	Electrical resistivity 10^{-4} Ωm
N - (AlGa)As	0.12	4.12
P - (AlGa)As	65.00	0.72
p - GaAs	2.00	2.02

The current spreading effect

In the calculations, the current spreading effect is taken into account. For diode lasers with a small lateral diffusion of carriers [32], the current density distribution at the p-n junction is assumed to be of the following form [33, 34]:

$$j(y) = \begin{cases} j_1 & \text{for } |y| \leq S/2 \\ j_1/[1 + (y - S/2)/10]^2 & \text{elsewhere} \end{cases} \tag{8}$$

with [35]:

$$j_1 = j + 2(B/S)^2 - 2(B/S)[(B/S)^2 + j]^{1/2} \tag{9}$$

$$j = I/LS \tag{10}$$

$$l_o = B(j_1)^{-1/2} \tag{11}$$

$$B = [2n_c kT/(\mathrm{Re})]^{1/2} \tag{12}$$

where I is the supply current, S is the stripe width, L is the resonator length,

R is the composite sheet resistance in the y direction (c. f. the coordinate system shown in Fig. 4):

$$\frac{1}{R} = \sum_i \frac{d_i}{p_i} \tag{13}$$

d_i is a thickness of the ith layer, p_i is its electrical resistivity, and the summation in (13) is carried out over all layers between the stripe contact and the active area; k is the Boltzmann constant, e is the unit charge and n_c is a constant (for DH GaAs/(AlGa)As diode lasers [36]: $n_c = 2$).

We assume the same relative distribution of the active area heat generation as for the p-n junction current density:

$$g_A(y) = g_A j(y)/j \tag{14}$$

Values of electrical resistivities are listed for the semiconductor layers of the laser in Table 4. We assume that Joule heating is insignificant in the remaining layers. The electrical resistivities have been calculated using formulas given in Reference [37].

Heat-sinking analysis

Heat spreading process in a heat sink of a diode laser plays an essential role in heating their active areas. During a cw operation, a participation of a heat sink temperature increase in the total temperature increase of a laser amounts to as much as one fifth to one third.

We use the thin-layer method of the calculations of the heat sink temperature increase. In this method proposed by Laff *et al.* [38], the effective width S_{EF} of a heat flux flowing into the heat sink is calculated in the following way

$$S_{EF} = (P / L\lambda_{TI})(\delta T_{AV} / \delta d_{TI})^{-1} \tag{15}$$

This procedure gives good accuracy when applied to layers which have little lateral heat flux spreading. Therefore it is used for the titanium bonding layer which is rather thin and has a relatively low thermal conductivity as compared with layers on either side. In Eq. (15), P is the dissipated power and δT_{AV} is the calculated change of the average active area temperature

which would follow the hypothetical change δd_{TI} of the T_i layer thickness of the thermal conductivity λ_{TI}.

The effective width S_{EF} is the width of a uniform heat flux which gives the same averaged active area temperature increase as the real heat flux. In its determination, we use the approximated formulas introduced on the basis of the formula (15) and given in Ref. [39]. For the considered structure the formula reduces itself to the following form:

$$S_{EF}[\mu m] = 31.9 + 0.339\{S[\mu m]\}^{1.35} \tag{16}$$

The heat sink temperature increase may be now expressed as follows:

$$\Delta T_{HS} = \Theta_{HS} q_{HS} S_{EF} L \tag{17}$$

where Θ_{HS} is the spreading thermal resistance of the heat sink and

$$q_{HS} = P/(S_{EF}L) \tag{18}$$

To determine the Θ_{HS} resistance, we use the formula of Joyce and Dixon [8]

$$\Theta_{HS} = [0.5 + 1n(2L/S_{EF})]/(\lambda_{HS}\pi L) \tag{19}$$

where λ_{HS} is the heat sink thermal conductivity (for copper, λ_{HS} = 400 W/mK [28]).

For the considered structure of the diffused-stripe diode laser, we obtain {c. f. Eq. (16)} the effective stripe width S_{EF} = 45.0 μm, which gives {c. f. Eq. (19)} the thermal heat spreading resistance of the heat sink Θ_{HS} = 6.72 K/W.

The dissipated power may be expressed as follows

$$P = q_{HS} S_{EF} L = U[I_{TH} + (I - I_{TH})(1 - a_E)] + I^2 R_s \tag{20}$$

where R_s is the series electrical resistance of the diode laser. This resistance may be determined with the aid of the following approximated formula

$$R_s = \sum_i p_i d_i / (LS) \tag{21}$$

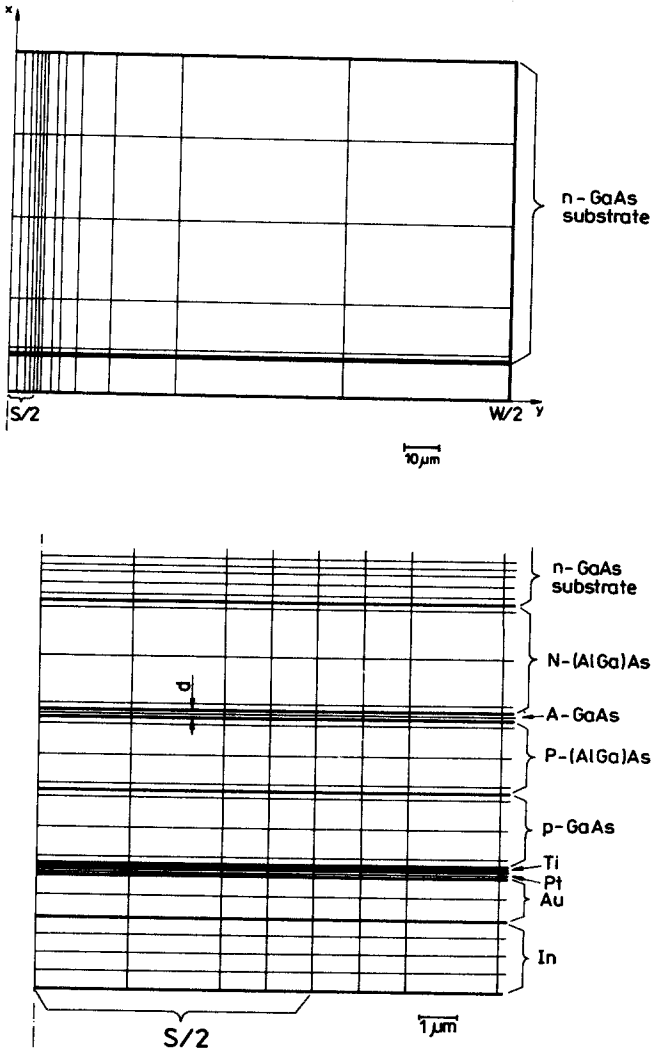

Fig. 6 The perpendicular grid used for the temperature calculations in the diffused-stripe diode laser: a) the whole laser structure, b) an enlarged neighbourhood of the active area

where p_i and d_i are in turn the electrical resistivity and the thickness of the ith layer. Taking the p_i values from Table 4 and the d_i values from Fig. 4, we get $R_S = 0.30\ \Omega$. For the nominal set of the supply data listed in Table 2, the dissipated power is hence equal to 1.34 W, and, from the equation (17), we obtain finally the heat sink temperature increase $\Delta T_{HS} = 9.0$ K.

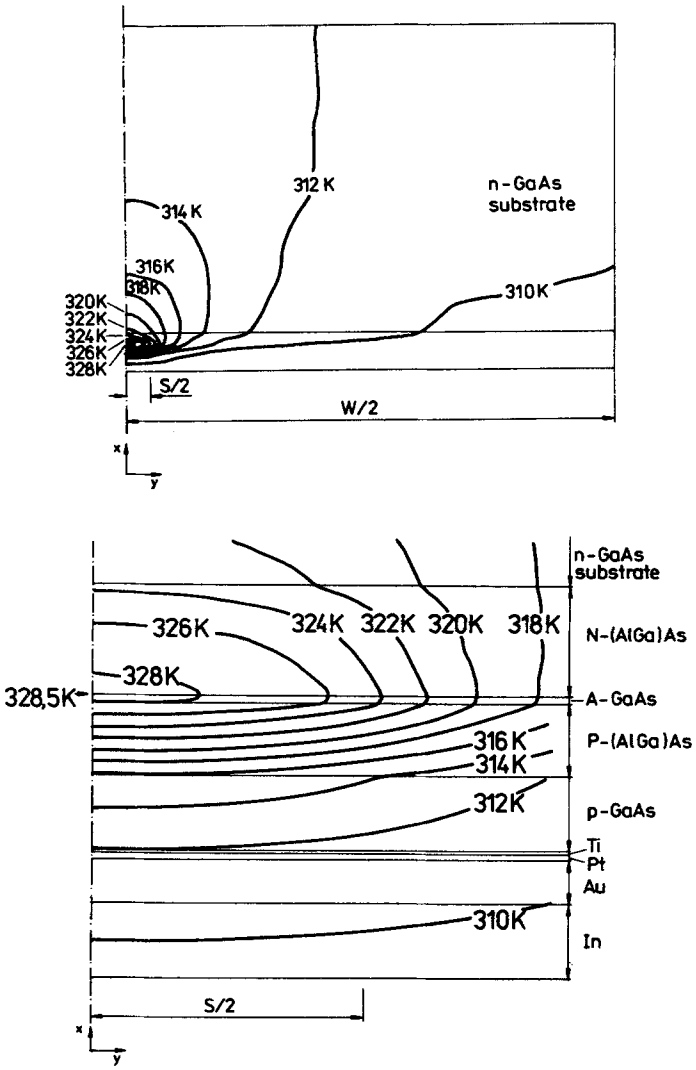

Fig. 7 Isothermal lines in the diffused-stripe diode laser: a) the whole laser structure, b) an enlarged neighbourhood of the active area. In the FEM temperature calculations, the heat-sink temperature increase $\Delta T_{HS} = 9.0$ K has been taken into account

The finite element thermal modelling

A half of the structure of GaAs/(AlGa)As diffused-stripe diode laser is covered with the perpendicular grid of 13x36 = 468 elements as shown in Fig. 6. Dimensions of elements used in the modelling are choosen purposly

in the way which ensures high accuracy of the thermal analysis. That is why the elements are much less in areas of relatively high temperature gradients, i. e. in a neighbourhood of the active area, than in regions far from it.

In the calculations, the heat sink temperature increases $\Delta T_{HS} = 9.0$ K (Section 3.3) is taken into account.

The CPU time required for the FEM analysis of the diffused-stripe diode laser amounts to only 120 to 180 seconds using the IBM PC/AT (6 MHz) microcomputer.

Isotherms

The FEM software module O.K.FOUR enables us to obtain immediately a system of isotherms for the structure under consideration. Such a system for the diffused-stripe GaAs/(AlGa)As diode laser is shown in Fig. 7. As one can see in this case the highest temperature increase ΔT_{MAX} takes place within the active area and amounts to as much as 28.5 K.

The isotherm configuration allows us to value relative participations of individual heat paths, i. e. it enables us to determine a shape, a direction and a relative density of individual heat fluxes. Along the x axis, a density of isotherms in the direction towards the heat sink is as much as 4 times higher than in the opposite direction. Corresponding heat fluxes are hence related to each other in the same ratio. On the other hand, the horizontal temperature gradient inside the active area is also four times lower than that inside the passive layer towards the heat sink but it should be noted that the thermal conductivity of the former area is much higher than that of the latter one. A curvature of isotherms in individual layers determines lateral heat spreading in those layers. All the above facts show in which a way a shape of isothermal lines enables us to determine the heat spreading process in the neighbourhood of the active area.

Temperature profiles

A temperature profile along the x axis is shown in Fig. 8. As one can see, temperature changes very quickly within the P-type and the N-type (AlGa)As passive layers. This corresponds to an increasing density of isotherms observed inside the above layers in Fig. 7b. [A convex shape of the temperature profile inside the N-type passive layer is a result of its relatively important local heat source [40] (c. f. Table 3)]. An analogous temperature profile calculated for the case when the current spreading effect has been neglected is plotted as a dashed line.

Horizontal temperature profiles, i. e. along the y axis, in the centres of individual layers are presented in Fig. 9. Temperature gradients in this direction within the (AlGa)As passive layers are slightly lower than that within the active layer in spite of their much lower thermal conductivity. On the other hand, temperature grandients in both the high-thermal-conductivity GaAs layers, i. e. the p-type capping layer and the lower part of the n-type substrate (*T* layer), are relatively low. It is an evidence of a less important lateral heat spreading mechanism in these layers. As in Fig. 8, the dashed line corresponds to the case without the current spreading effect.

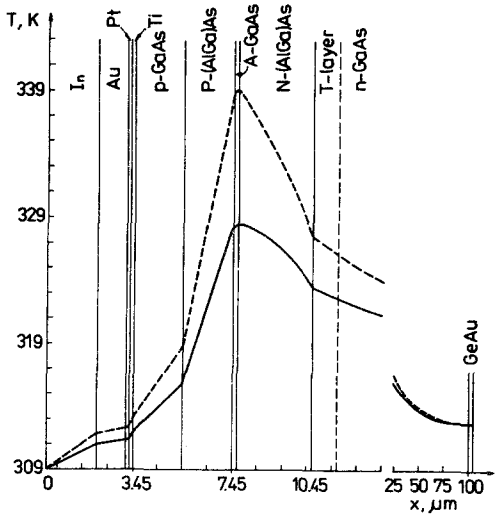

Fig. 8 The temperature profile along the x axis for the diffused-stripe diode laser. The profile plotted with a dashed line corresponds to the case without a current spreading effect

Both the above figures, i. e. Figs 8 and 9, show us what a mistake in the temperature calculations is made when the current spreading effect is neglected (c. f. corresponding solid and dashed lines).

A relative participation of individual heat sources in stripe-geometry diode lasers may be discussed on the basis of plots shown in Fig. 10. It is seen a surprisingly important contribution of the Joule heating (especially in the N-type (AlGa)As passive layer) in the whole heating process. This contribution is even comparable with that of the active area heating whose generation rate is much higher, but the generation volume much less (c. f. heat powers in Table 3). But one should call the reader's attention to the

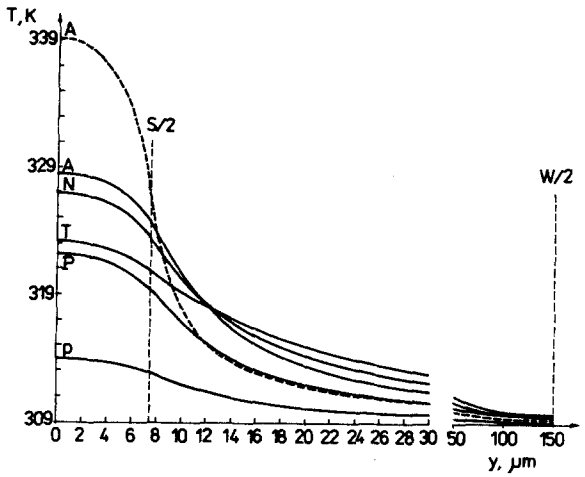

Fig. 9 The temperature profiles along the y axis in the centres of individual layers; A - active layer, N - N-type (AlGa)As layer, P - P-type (AlGa)As layer, p - p-type capping GaAs layer, T - lower part of the substrate absorbing the spontaneous radiation. The dashed line corresponds to the active-layer horizontal profile for the case without current spreading

fact that the Joule heating generation rates are proportional to the second power of the supply current, whereas the remaining rates only to the first power. Therefore for such a high excitation level as considered in the present work (I = 1A *vs.* I_{TH} = 0.1 A) their contribution should be considerable. For lower supply currents their importance would be less than that of the heat sources connected with absorption of spontaneous radiation beyond the active area [11]. When we neglect the local heat source in the N-type (AlGa)As layer, i. e. the Joule heating within this layer, temperature profiles stop being convex there (c. f. curves A, A + Tn an A + T).

Plots in Fig. 10 enable us also to compare results of our FEM thermal analysis with those obtained with the aid of the semi-analytical model of Joyce and Dixon [8] (JD model). For the laser structure under consideration, the highest active-area temperature increase ΔT_{JD} calculated by means of the version of the JD model prepared by Newman *et al.* [1] amounts to 30.5 K. In the above calculations, the current spreading effect and the Joule heating have been neglected. After recalculating our results for this case, we obtain ΔT_S = 29.1 K. This value seems to be in a good agreement with that of the JD model.

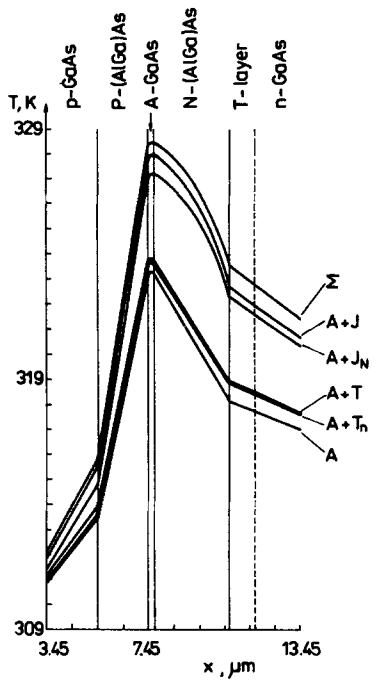

Fig. 10 The temperature profiles along the x axis for various heat sources taken into account; A - active layer heating, T_n - absorption of the spontaneous radiation in the lower part of the substrate, T - absorption of the above radiation in both the lower part of the substrate and the p-GaAs capping layer, J_N - Joule heating in the N-type (AlGa)As layer, J - Joule heating in both the P-type and the N-type (AlGa)As layers and Σ - all heat sources

On the other hand, the above ΔT_S value is very close to the ΔT_{MAX} exact value of this temperature increase shown e. g. in Fig. 7. That means that in our peculiar case influences of both the processes which had been neglected in the JD model, i. e. the Joule heating and the current spreading, compensate each other. But this is a case only for that pecular laser structure and that specified supply condition. Usually the above simplifications lead to considerable errors in temperature calculations in diode lasers.

Conclusions

In the present work, the finite element technique has been tested for the use in a thermal analysis of stripe-geometry diode lasers. This method appears to be very exact and surprisingly speed.

As an example, a finite element thermal analysis of the diffused-stripe double-heterostructure GaAs/(AlGa)As diode laser has been carried out. For the diode laser whose an active area is of the dimensions: 0.2 μm x 15 μm x 400 μm, supplied with the current 1 A, the maximal temperature increase is placed in its active area and amounts to 28.5 K. A density of the heat flux from the active area directly towards the heat sink appears to be as much as 4 times greater than that in the opposite direction. For such a high values of the supply current, the Joule heating plays a considerable role in the whole heating process. The current spreading effect is also of significant importance.

* * *

The work was carried out under the Polish Central Program for Fundamental Research, CPBP 01.06, 6.04.

References

1 D. H. Newman, D. J. Bond and J. Stefani, Solid-State Electr. Dev. 2 (1978) 41.
2 J. Buus, IEEE J. Quantum Electron., QE-15 (1979) 734.
3 E. Duda, J. C. Carballes and J. Apruzzese, IEEE J. Quantum Electron., QE-15 (1979) 812.
4 A. G. Steventon, R. E. Spillett, R. E. Hobbs, M. G. Burt, P. J. Fiddyment and J. V. Collins, IEEE J. Quantum Electron., QE-17 (1981) 602.
5 M. Yano, H. Iami, K.-I. Hori and M. Takusagawa, IEEE J. Quantum Electron., QE-17 (1981) 619.
6 M. Ito and T. Kimura, IEEE J. Quantum Electron., QE-17 (1981) 787.
7 T. J. S. Mattos, N. B. Patel and F. D. Nunes, J. Appl. Phys., 53 (1982) 149.
8 W. B. Joyce and R. W. Dixon, J. Appl. Phys., 46 (1975) 855.
9 W. Nakwaski, Optica Applicata, 13 (1983) 281.
10 W. Nakwaski, IEE Proc. - J (Optoelectronics), 134 (1987) 87.
11 W. Nakwaski, IEE Proc. - I (Solid-State and Electron Devices), 131 (1984) 94.
12 P. Enders and J. Gailey, Kvantovaya Elektronika, 15 (1988) 2253 (in Russian).
13 T. Kobayashi and G. Iwane, Jpn. J. Appl. Phys., 16 (1977) 1403.
14 J. Manning, J. Appl. Phys., 52 (1981) 3179.
15 P. A. Morton, M. S. Demokan and R. F. Ormondroyd, submitted to IEE Proc. - J (Optoelectronics).
16 R. Papannareddy, W. Ferguson and J. K. Butler, J. Appl. Phys., 62 (1987) 3565.
17 J. Piprek and R. Nuernberg, Kvantovaya Elektronika, 15 (1988) 2249 (in Russian).
18 O. C. Zienkiewicz, The Finite Element Method, McGraw-Hill, London, 1977.
19 W. Nakwaski, Optica Applicata, 13 (1983) 513.
20 W. Nakwaski, Sci. Bull. Lodz Techn. Univ., 469 (Physics-8) (1985) 15.
21 W. Engeler and M. Garfinkel, Solid-State Electron., 8 (1965) 585.

22 M. A. Afromowitz, J. Appl. Phys., 44 (1973) 1292.
23 S. Adachi, J. Appl. Phys., 54 (1983) 1844.
24 W. Nakwaski, J. Appl. Phys., 64 (1988) 159.
25 I. Hayashi, M. B. Panish and F. K. Reinhart, J. Appl. Phys., 42 (1971) 1929.
26 H. Kressel and M. Ettenberg, J. Appl. Phys., 47 (1976) 3533.
27 J. C. Dyment and L. A. D'Asaro, Appl. Phys. Lett., 11 (1967) 292.
28 D. E. Gray (Ed.), American Institute of Physics Handbook, McGraw-Hill, New Jork 1972, Table 4g-8.
29 T. Kobayashi and Y. Furukawa, Jpn. J. Appl. Phys., 14 (1975) 1981.
30 W. Nakwaski, Sov. J. Quantum Electron, (USA), 9 (1979) 1544 [see also: Kvantovaya Elektronika, 6 (1979) 2609 (in Russian)].
31 H. C. Casey, Jr., D. D. Sell and M. B. Panish, Appl. Phys. Lett., 24 (1974) 63.
32 W. B. Joyce, J. Appl. Phys., 51 (1980) 2394.
33 W. B. Joyce and S. H. Wemple, J. Appl. Phys., 41 (1970) 3818.
34 W. B. Dumke, Solid-State Electron., 16 (1973) 1279.
35 J. Buus, PhD Thesis, Electromagnetics Institute, Technical University of Denmark, Lyngby 1973, p. 31.
36 C. H. Henry, R. A. Logan and F. R. Merritt, J. Appl. Phys., 49 (1978) 3530.
37 W. Nakwaski, Optica Applicata, 19 (1989) in print.
38 R. A. Laff, L. D. Comerford, J. D. Crow and M. J. Brady, Appl. Opt., 17 (1979) 778.
39 W. Nakwaski, J. Thermal Analysis, in print.
40 W. Nakwaski, Optica Applicata, 13 (1983) 115.

Zusammenfassung — Es wurde die Anwendbarkeit der Elementenmethode bei der Thermoanalyse von Diodenlaser des Streifentypes dargestellt. Dieses Verfahren zeigte sich als sehr genau und unter Anwendung eines IBM PC/AT der Standardausführung auch als überraschend schnell.

Als Beispiel wurde die Elementenmethode bei der Thermoanalyse eines doppelt heterostrukturellen GaAs/(AlGa)As Diodenlasers vom Diffusionsstreifentyp durchgeführt. Eine für den obengenannten Laser erhaltene Schar von Isothermen ermöglicht die Diskussion der Wärmeausdehnung innerhalb der Konstruktion sowie den Vergleich der relativen Beiträge aller Wärmequellen.